

The aggregation-induced emission enhancement properties of BF_2 complex isatin-phenylhydrazone: Synthesis and fluorescence characteristics



Jie Zheng ^a, Fang Huang ^b, Yujin Li ^{a,*}, Tianwei Xu ^a, Hui Xu ^a, Jianhong Jia ^a, Qing Ye ^a, Jianrong Gao ^{a,**}

^a State Key Laboratory Breeding Base of Green Chemistry-Synthesis Technology, Zhejiang University of Technology, Hangzhou 310014, People's Republic of China

^b Department of Pharmacology, School of Pharmaceutical Sciences, Southern Medical University, Guangzhou 510515, People's Republic of China

ARTICLE INFO

Article history:

Received 16 June 2014

Received in revised form

13 September 2014

Accepted 17 September 2014

Available online 28 September 2014

Keywords:

AIEE

Isatin-phenylhydrazone dyes

Boron complexes

Fluorescent dyes

Solid state

Synthesis

ABSTRACT

Isatin-phenylhydrazone derivatives and their corresponding BF_2 complexes were efficiently synthesised by a three-step reaction starting from isatin and phenylhydrazine hydrochloride. The fluorescence properties of the isatin-phenylhydrazone derivatives and derived BF_2 complexes were investigated in different organic solvents, in the solid state and in mixed solvent solutions of THF and H_2O . These fluorescent dyes exhibited low fluorescent intensity in solution but a high fluorescent intensity as aggregates and in their solid state due to the interesting aggregation-induced emission enhancement characteristics which were caused by the inhibition of intramolecular rotation in the single molecule state. Information supporting this inference was supported by single crystal X-ray analysis.

© 2014 Published by Elsevier Ltd.

1. Introduction

BF_2 complexes are known as fluorescent dyes: they exhibit high fluorescence quantum yield, excellent photostability and sharp fluorescence spectra [1] and are often applied to electrochromic display systems [2], solar cells [3], liquid crystals [4], optical storage devices [5] and laser dyes [6]. Solid state emissive BF_2 complex dyes, in particular, have garnered much attention from many research groups because of their fundamental importance and practical applications in optoelectronic devices such as: field-effect transistors [7], live-cell imaging [8], organic light-emitting diodes (OLEDs) [9], and fluorescent sensors [10]. In 2001 Tang's group first reported that the luminescence of silole molecules was stronger in the aggregate state than that in the solution state [11] because of the phenomenon of aggregation-induced emission

enhancement (AIEE) [12], which is now attracting increasing research attention. These compounds which have the AIEE characteristics exhibit weak luminescence or have almost no emissions in their solution state, but show highly emissive behaviour in their aggregated and solid states. Only a limited number of organic fluorescent dyes have been reported as displaying AIEE characteristics, these include for example: 1,4-di[(E)-2-phenyl-1-propenyl]benzene (PPB) [13], siloles [11b,14], thienylazulene [15], arylethene derivatives [16] and salicylaldehyde azine derivatives [17]. Therefore exploration of new AIEE fluorophores remains of interest.

However, most boron complexes hardly fluoresce in the solid state owing to the formation of delocalised excitons or excimers, which may cause enhanced non-radiative deactivation of the excited state [18], better known as aggregation-caused quenching (ACQ) [19]. In our current work readily synthesised boron fluoride complexes of isatin-phenylhydrazone were found to exhibit good AIEE characteristics. The results showed that isatin derivatives and their BF_2 complexes displayed attractive luminescent properties in the solid state and were induced to emit intense fluorescence with aggregate formation.

* Corresponding authors. Tel.: +86 0571 88320891.

** Corresponding author.

E-mail address: lyjzjut@zjut.edu.cn (Y. Li).

2. Experimental

2.1. General

All of the chemicals used in the current study were purchased from commercial vendors and used as received without further purification, unless otherwise noted. All solvents were purified and dried using standard methods prior to use. Fourier transform-infrared (FTIR) spectra were performed using Thermo Nicolet 6700 spectrophotometer. Nuclear magnetic resonance (^1H , ^{13}C and ^{19}F NMR) spectra were recorded on a Bruker AM 500 spectrometer (Bruker) with chemical shifts reported as ppm at 500, 125 and 376 MHz, respectively, (in CDCl_3 , TMS as internal standard). Fluorescence spectra were obtained with a F-7000 Fluorescence Spectrophotometer in a solution of 100 μM . UV–Vis absorption spectra were measured on a UV-2550.

2.2. Preparation of compounds **1a**–**1b**

A mixture of isatin (10.0 mmol, 1.4722 g), ethyl bromide (10.0 mmol, 1.0905 g) and anhydrous K_2CO_3 (14.5 mmol, 2.0 g) in DMF (10 mL) was stirred vigorously for 12 h at room temperature and complete reaction was detected by TLC analysis. The reaction mixture was poured into water (100 mL) and the precipitate was concentrated to give crude product and recrystallized from EtOH [20].

2.2.1. 1-ethylindole-2,3-dione (compound **1a**)

Red solid. Yield 1.7110 g, 98%. Mp: 91–92 °C (ref: 94 °C) [20]. GC–MS: 175.0.

2.2.2. 1-benzylindole-2,3-dione (compound **1b**)

From isatin and benzyl chloride as an orange-yellow solid. Yield 2.3467 g, 99%. Mp: 132–133 °C (ref: 132 °C) [21]. GC–MS: 237.0.

2.3. Preparation of compounds **2a**–**2b**

A mixture of **1a** (5.0 mmol, 0.8755 g), phenylhydrazine hydrochloride (5.0 mmol, 0.7325 g) in DMF (10 mL) was stirred vigorously at room temperature overnight. The reaction mixture was poured into water (100 mL) and extracted with ethyl acetate (3 × 20 mL). The combined organic layer was dried with MgSO_4 and the solvent was removed under reduced pressure. The residue was purified by silica gel chromatography eluting (silica gel, ethyl acetate: petroleum ether = 1:5) leading to phenylhydrazone derivative **2a** as a yellow solid [22].

2.3.1. 1-ethylindole-3-phenylhydrazone (compound **2a**)

Yellow solid. Yield 0.8220 g, 62%. Mp: 78–79 °C. ^1H NMR (500 MHz, CDCl_3) δ 12.83 (s, 1H), 7.68 (d, 1H, J = 7.5 Hz), 7.38–7.37 (m, 4H), 7.31–7.29 (m, 1H), 7.14–7.11 (m, 1H), 7.08–7.05 (m, 1H), 6.93 (d, 1H, J = 7.9 Hz), 3.89 (q, 2H, J = 7.3 Hz), 1.35 (t, 3H, J = 7.3 Hz). GC–MS: 265.0.

2.3.2. 1-benzylindole-3-phenylhydrazone (compound **2b**)

Yellow solid. Yield 1.3566 g, 83%. Mp: 138–139 °C. ^1H NMR (500 MHz, CDCl_3): δ 12.84 (s, 1H) 7.69 (d, 1H, J = 7.3 Hz) 7.68–7.37

(m, 4H), 7.36–7.30 (m, 4H), 7.30–7.28 (m, 1H), 7.22–7.13 (m, 1H), 7.13–7.07 (m, 2H), 6.82 (d, 1H, J = 7.9 Hz), 5.02 (s, 2H). ^{13}C NMR (125 MHz, CDCl_3): δ 162.27 (2C), 142.63 (1C), 140.18 (1C), 135.83 (1C), 129.46 (2C), 128.88 (2C), 127.96 (1C), 127.75 (1C), 127.29 (2C), 126.76 (1C), 123.29 (1C), 122.67 (1C), 121.46 (1C), 118.95 (1C), 114.42 (1C), 109.35 (1C), 43.24 (1C).

2.4. Preparation of compounds **3a**–**3b**

To a stirred solution of **2a** (0.5 mmol, 0.1328 g) in degassed anhydrous dichloromethane (20 mL), Et_3N (10 mmol, 1.5 mL) was syringed under nitrogen atmosphere. After stirred for 20 min, $\text{BF}_3 \cdot \text{OEt}_2$ (10 mmol, 1.25 mL) was successively added by syringe. The mixture was stirred at room temperature overnight and complete reaction was detected by TLC. The mixture was quenched with water (20 mL), and extracted with dichloromethane (3 × 20 mL). The organic layer was dried with MgSO_4 and the solvent was removed under reduced pressure. The residue was purified by silica gel chromatography eluting (silica gel, ethyl acetate: petroleum ether = 1:10) to afford clean complex **3a** as a orange-yellow solid.

2.4.1. 5-ethyl-3,3-difluoro-2-phenyl-3,5-dihydro-2*H*-[1,3,4,2]oxadiazaborinino[6,5-*b*]indol-4-iium-3-uide (compound **3a**)

Orange-yellow solid. Yield 0.1253 g, 80%. Mp 163–166 °C. FTIR (KBr, cm^{-1}) 2987.2, 1608.4, 1508.5, 1321.0, 1282.5, 1210.1, 1135.9, 1023.3, 761.8, 545.8, 432.0. ^1H NMR (CDCl_3 , 500 MHz): δ 7.90–7.88 (m, 1H), 7.85–7.83 (m, 2H), 7.47–7.44 (m, 2H), 7.40–7.39 (m, 2H), 7.39–7.36 (m, 1H), 7.35–7.26 (m, 1H), 4.19 (q, 2H, J = 7.4 Hz), 1.53 (t, 3H, J = 7.4 Hz). ^{13}C NMR (CDCl_3 , 125 MHz): δ 152.84 (1C), 145.16 (1C), 136.02 (1C), 128.94 (2C), 126.85 (1C), 126.54 (1C), 124.88 (1C), 123.29 (1C), 121.56 (1C), 120.72 (1C), 119.01 (2C), 110.74 (1C), 36.72 (1C), 13.45 (1C). ^{19}F NMR (CDCl_3 , 376 MHz): δ –130.94 (s, 1F), –131.00 (s, 1F). HRMS (ESI-TOF) found: $[\text{M} + \text{H}]^+$ 314.1273, molecular formula $\text{C}_{16}\text{H}_{14}\text{BF}_2\text{N}_3\text{O}$, requires $[\text{M} + \text{H}]^+$ 314.1271.

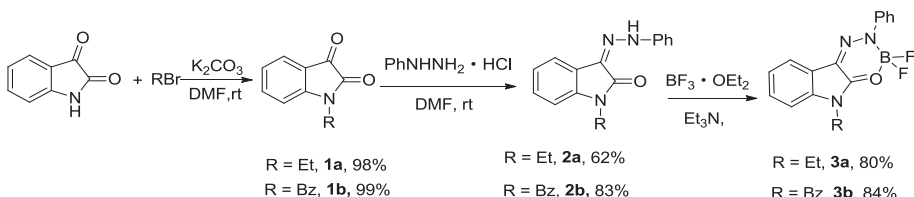
2.4.2. 5-benzyl-3,3-difluoro-2-phenyl-3,5-dihydro-2*H*-[1,3,4,2]oxadiazaborinino[6,5-*b*]indol-4-iium-3-uide (compound **3b**)

Deep-yellow solid. Yield 0.3758 g, 84%. Mp: 145–149 °C. FTIR (KBr, cm^{-1}) 3060.5, 1634.0, 1508.1, 1458.1, 1266.7, 1183.4, 1133.0, 1023.8, 881.3, 757.9, 555.4. ^1H NMR (500 MHz, CDCl_3): δ 7.89–7.86 (m, 3H), 7.48 (t, 2H, J = 1.9 Hz), 7.45–7.28 (m, 8H), 7.17 (d, 1H, J = 7.4 Hz), 5.27 (s, 2H). ^{13}C NMR (125 MHz, CDCl_3): δ 153.14 (1C), 145.20 (1C), 136.28 (1C), 133.48 (1C), 129.30 (2C), 128.92 (2C), 128.72 (1C), 127.67 (2C), 127.11 (1C), 126.59 (1C), 125.03 (1C), 123.13 (1C), 121.58 (1C), 120.90 (1C), 118.95 (1C), 114.46 (1C), 111.62 (1C), 45.52 (1C). ^{19}F NMR (CDCl_3 , 376 MHz): δ –130.96 (s, 1F), –131.02 (s, 1F). HRMS (ESI-TOF) found: $[\text{M} + \text{H}]^+$ 376.1436, molecular formula $\text{C}_{21}\text{H}_{16}\text{BF}_2\text{N}_3\text{O}$, requires $[\text{M} + \text{H}]^+$ 376.1427.

3. Results and discussion

3.1. Synthesis

Preparation of the substituted isatin-phenylhydrazone derivatives (precursor **2**) and their corresponding boron complexes (BODIHY **3**) is shown in Scheme 1. To inhibit the H atom on the N



Scheme 1. The synthesis of the precursor **2** and the BODIHY **3**.

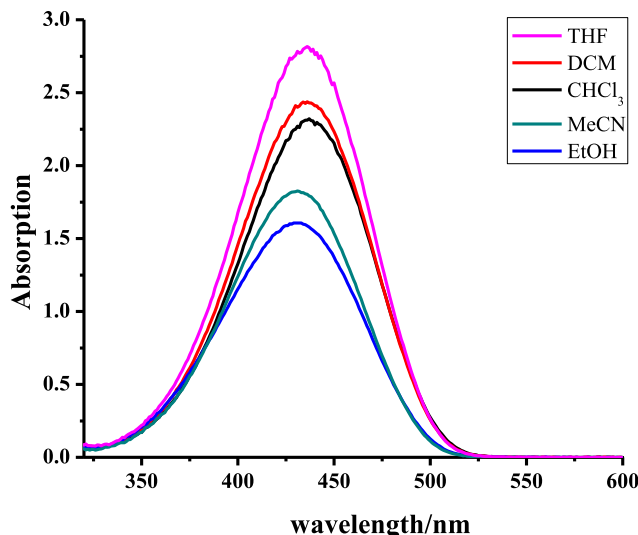


Fig. 1. Absorption spectra of compound **3b** (100 μ M) in different Solution (PMT Voltage: 900 V).

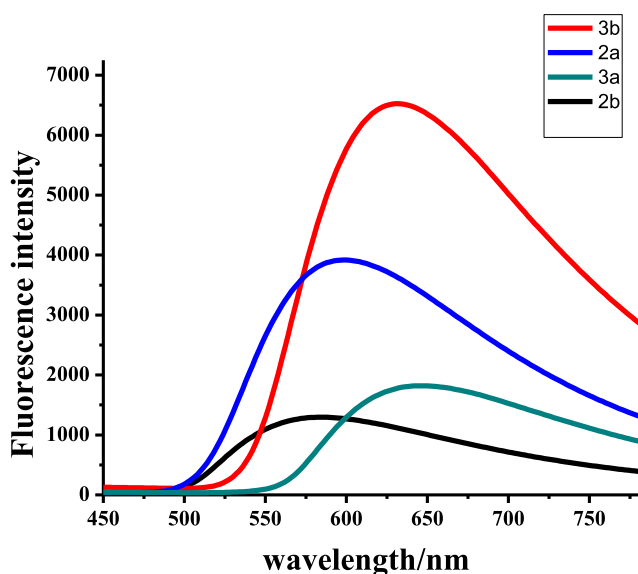


Fig. 2. Fluorescence emission spectra of the precursor **2** ($\lambda_{\text{ex}} = 400$ nm) and the BODIHY **3** ($\lambda_{\text{ex}} = 435$ nm) in the solid state (PMT Voltage: 600 V).

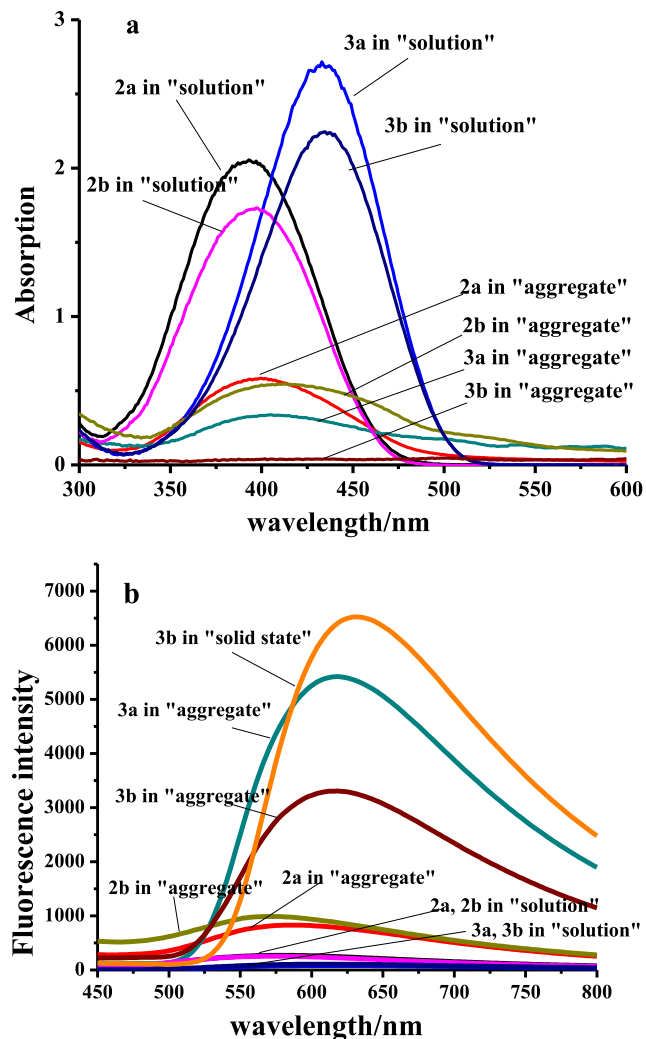


Fig. 4. Absorption (a) and fluorescence emission spectra (b) of the precursor **2** ($\lambda_{\text{ex}} = 400$ nm) (100 μ M) and the BODIHY **3** ($\lambda_{\text{ex}} = 435$ nm) (100 μ M) in THF solution and "aggregate" (THF/water, 1:9, v/v) states (PMT Voltage: 900 V).

atom in the isatin which will affect the reaction, a series of substituents (ethyl, benzyl) were introduced at first as electron-donating groups and also to act as bulky steric groups. The N-alkylation isatin was accomplished by the reaction of isatin and

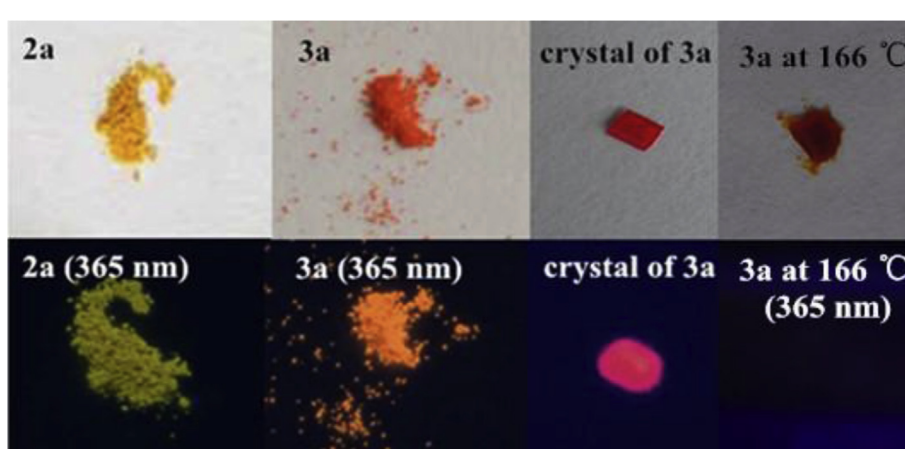


Fig. 3. The colour of compound **2a** and **3a** in the solid state and crystal. (For interpretation of the references to colour in this figure legend, the reader is referred to the web version of this article.)

alkyl bromide in the presence of K_2CO_3 (1.4 equiv.) in DMF at room temperature; precursor **2** was prepared by condensation of the isatin derivative with phenylhydrazine hydrochloride (1 equiv.) in DMF at room temperature which resulted in a 62% (**2a**) and 83% (**2b**) yield. The BODIHY **3** was produced, with a yield of 80% (**3a**) and 84% (**3b**) yield, by using an excess of $BF_3 \cdot OEt_2$ in DCM with Et_3N as the base and purification by column chromatography (silica gel, EA: PE = 1:10). The structures of the boron complexes were fully characterised by FTIR, 1H NMR, ^{13}C NMR, GC-MS, and HRMS analysis.

3.2. Fluorescence properties

The fluorescence properties of **2a**, **2b**, **3a**, and **3b** were examined under different conditions such as: in different organic solvents, in their solid states, and in a mixture in solution of THF and H_2O . The AIEE characteristics of **2a**, **2b**, **3a**, and **3b** were investigated in THF/water (from 10:0 to 1:9, v/v) and shown in Figs. 5 and 6. Optical data in different solutions for all compounds are gathered in Table 1.

3.2.1. Fluorescence in solution

The solvent effect on the absorption and fluorescence properties of phenylhydrazone derivatives (**2a**, **2b**) and their corresponding boron complexes (**3a**, **3b**) were examined (see Fig. 1, Table 1). As shown in Fig. 1 and Table 1, the precursor **2** showed a sharp

absorption peak at approximately 400 nm along with a vibrational peak. The maximum absorption wavelength (λ_{max}) of BODIHY **3** (435 nm) was more bathochromic than the precursor **2** (400 nm) and the λ_{max} of these compounds were barely affected by solvent polarity, suggesting that the dipole moments of the molecules in their ground and excited states were almost equal [23]. The molar absorption coefficient (ϵ) of BODIHY **3** underwent a slight change in different organic solvents and had the highest value in THF which was its best solvent. The fluorescence quantum yields (Φ_f) of BODIHY **3** were below 0.01 in organic solvents so these compounds hardly exhibited fluorescence in solution.

3.2.2. Fluorescence in the solid state

As shown in Fig. 2, although BODIHY **3a**, **3b** and their precursor phenylhydrazone **2a**, **2b** all exhibited AIEE, in BODIHY **3a**, **3b** the effect was more apparent than precursor **2** in their aggregate or solid states. The BF_2 complex **3** displayed a red shift (c. 50 nm) compared with precursor **2**, **2a** (598 nm), **3a** (646 nm), **2b** (584 nm), and **3b** (632 nm) (see Table 1). The complexation of BF_2 enhanced the molecular rigidity and coplanarity of BODIHY **3**, which caused the red shift. The colour of precursor **2a** and BODIHY **3a** in their solid state and the crystals of **3a** by direct visualization and UV lamp (365 nm) are shown in Fig. 3. Under UV black light excitation ($\lambda_{ex} = 365$ nm), precursor **2a** appeared green and BODIHY **3** appeared bright orange-red while the natural colour of **2a** was

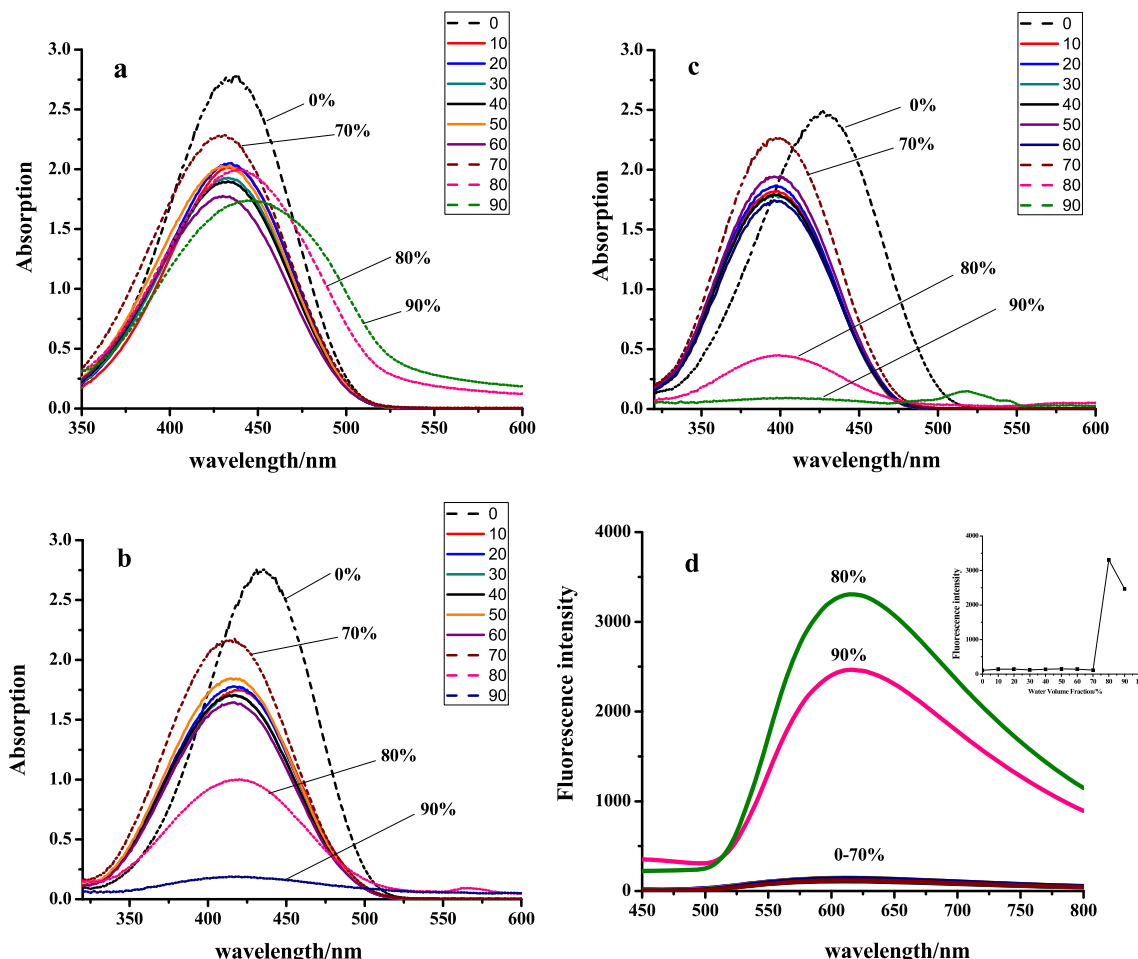


Fig. 5. Absorption (a, b, c) of dilute solution of compound **3b** (100 μ M) with different duration for 0 h (a), 1 h (b), 24 h (c) and fluorescence spectra (d) of compound **3b** (100 μ M) with duration for 3 h in THF/water mixtures with different water contents. Inset shows fluorescence titration curve of compound **3b** in the THF/water mixtures ($\lambda_{ex} = 435$ nm, PMT Voltage: 900 V).

orange and **3a** was red. Crystalline **3a** appeared bright rose-pink with a visible red shift under the UV lamp (365 nm) due to the different molecular stacking of the powdered and crystalline forms. Moreover, no fluorescence could be observed under the UV lamp (365 nm) when BODIHY **3a** was in its molten state at a temperature greater than 166 °C: this may have been due to the destruction of the configuration of **3a** as it melted at which point it could undergo free intramolecular rotation.

3.2.3. Fluorescence in the aggregated state

The AIEE characteristics of compounds **2a**, **2b**, **3a**, and **3b** were investigated in a mixture of THF and water (see Fig. 4). In THF compounds **2a** and **2b**, **3a**, and **3b** were well-dispersed and displayed structured absorption spectra and weak fluorescence emissions in their solution state. However, when they were in a poor solvent (THF/water (1:9, v/v)), no absorption in the visible region of their absorption spectra clearly suggested the formation of an aggregated state, and strong fluorescence emission was observed consequently with the maximum fluorescence wavelengths (F_{\max}) of precursor **2** at about 580 nm and that of BODIHY **3** at about 620 nm. In comparison, the AIEE effect of BODIHY **3** was much stronger than that of the precursor **2**.

To determine whether precursor **2** and BODIHY **3** have AIEE characteristics, the UV–Vis absorption spectra and fluorescence spectra of compound **3b** were measured in a series of THF/water mixtures with different volume fractions of water, since compound **3b** was soluble in THF but not in water (see Fig. 5). Compared with the UV–Vis spectrum of compound **3b** in different mixtures of THF and water over different test durations (quasi-instantaneous, 1 h, and 24 h), the maximum absorption wavelength and intensity were practically unchanged in the dilute THF solution (435 nm). However, an obvious blue shift (c. 35 nm) in the maximum absorption peak (435 nm (quasi-instantaneous), 420 nm (1 h), and 400 nm (24 h)) was observed when water was added (10–70% (v/v)) gradually, but the intensity underwent no significant change. When the water fraction was between 80 and 90%, the maximum absorption peak had the same blue shift, along with a rapidly decreased absorption intensity until this levelled-off to a tail (90%) in the visible region of their absorption spectra (see Fig. 5(a–c)). This phenomenon of the absorption intensity rapidly decreased with the increase of the water fraction may have been due to Mie scattering caused by nanoparticles [24]. Upon photoexcitation (see Fig. 5(d)), the dilute THF solution of compound **3b** showed a fluorescence spectrum with an emission peak at 604 nm despite its luminogen concentration remaining unchanged at 1×10^{-4} M over

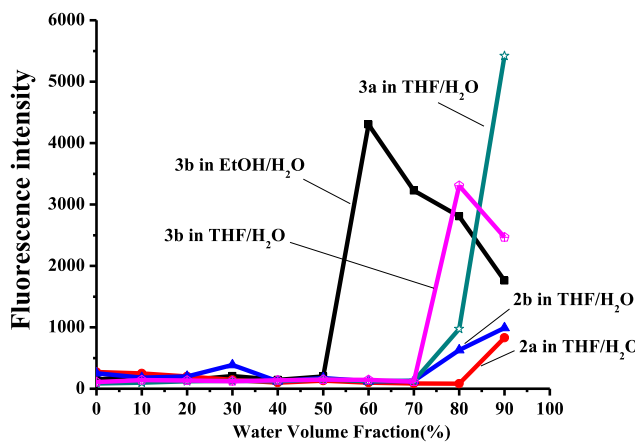


Fig. 6. Effect of water volume fraction on the AIEE fluorescence intensity (peaks in fluorescence spectra) of the precursor **2** ($\lambda_{\text{ex}} = 400$ nm) (100 μM) and the BODIHY **3** ($\lambda_{\text{ex}} = 435$ nm) (100 μM) in THF/water. (PMT Voltage: 900 V).

Table 1
Optical data measured in different solutions.

Dye	Matrix	λ_{abs} (max) (nm)	ϵ ($\text{M}^{-1} \cdot \text{cm}^{-1}$)	λ_{em} (max) (nm)
2a	CHCl ₃	402	21,670	584
	Solid			598
2b	CHCl ₃	403	19,260	568
	Solid			584
3a	CHCl ₃	437	26,590	620
	DCM	435	26,900	612
	THF	433	27,160	612
	EtOH	432	27,560	612
	MeCN	429	27,230	608
	Solid			646
	CHCl ₃	437	23,220	606
	DCM	435	24,470	618
	THF	435	28,170	604
3b	EtOH	430	16,090	604
	MeCN	431	18,260	602
	Solid			632

the 3 h test duration. Increasing the water content to 70% (v/v) in the solution containing **3b**, the fluorescence properties were almost the same until the water content reached 70% (v/v), because compound **3b** was soluble in the THF/water mixtures at a lower water content (≤ 70 (v/v)). However, as the water content increased to over 80% (v/v) in the THF/water mixture, the fluorescence intensity dramatically increased: the absorption intensity decreased rapidly (80–90%). Similar results were observed for compounds **2a**, **2b**, and **3a**. Since water was a poor solvent for compounds **2a**, **2b**, **3a**, and **3b**, the molecules of these compounds must have aggregated in the THF/water mixture system at those higher water contents (80–90% (v/v)). Therefore, the BODIHY **3a**, **3b** and their precursor phenylhydrazone **2a**, **2b** were AIEE active. More interestingly, according to

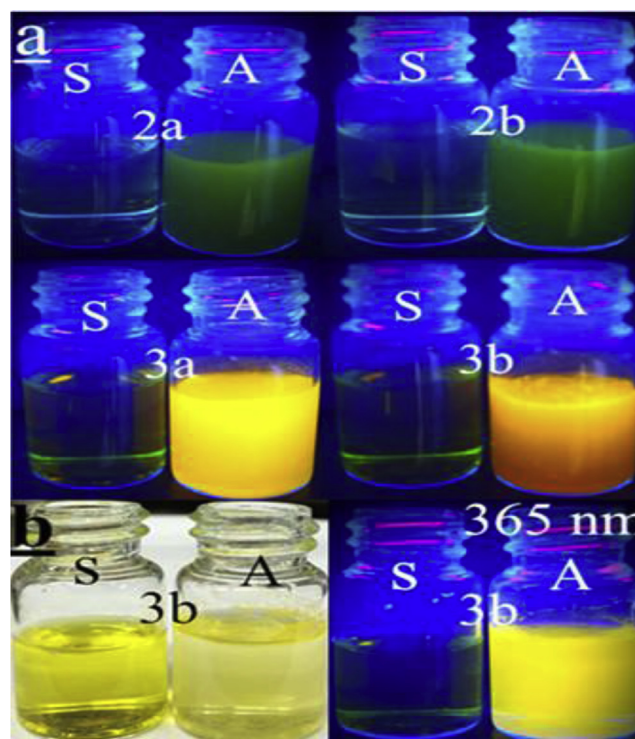


Fig. 7. (a) The colour of compound **2a**, **2b**, **3a** and **3b** under the UV lamp (365 nm), S = THF solution, A = aggregate (THF:water = 1:9, v/v). (b) The colour of compound **3b** under the naked eye and the UV lamp (365 nm). S = EtOH solution, A = aggregate (EtOH: water = 4:6, v/v). (For interpretation of the references to colour in this figure legend, the reader is referred to the web version of this article.)

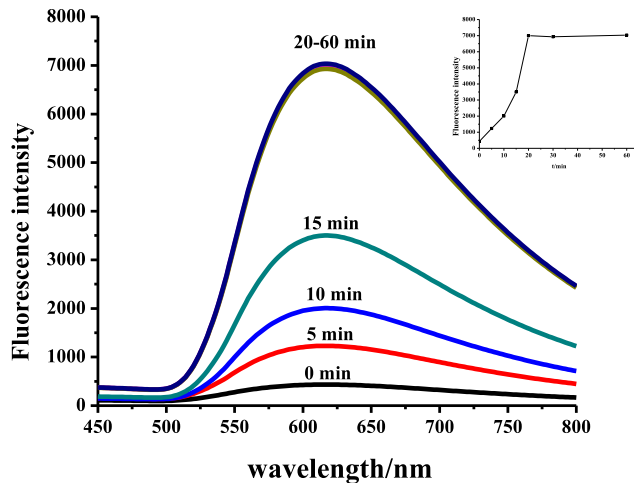


Fig. 8. Dependence of the fluorescence intensity of compound **3a** (100 μM) to aggregating time in THF/water (1:9, v/v). Inset shows fluorescence titration curve of compound **3a** to aggregating time in THF/water (1:9, v/v) ($\lambda_{\text{ex}} = 435 \text{ nm}$, PMT Voltage: 900 V).

the different solubilities of the compounds in the solvent, an AIEE effect also occurred at different volume fractions (see Fig. 6), such as compound **3b** for which this occurred at 70% volume fraction of water in the THF/water mixtures and 50% in the EtOH/water mixtures due to the better solubility in THF than in EtOH. With further increased water content to greater than 80% in the THF/water mixtures and 60% in the EtOH/water mixtures, the fluorescence of **3b** will be decreased due to precipitation. The AIEE effect occurred at 70% volume fraction of water for **2b** and **3a**, but at 80% for **2a** in the THF/water mixtures. This phenomenon was observed under the UV lamp (365 nm) (see Fig. 7).

To investigate the process of this AIEE phenomenon further, the relationship between the fluorescence intensity of compound **3a** and the aggregating time in the THF/water mixtures at 90% volumetric water content was studied. The mixture solutions of **3a** were configured by water which was immediately added to the THF solution of **3a** and ultrasonicated (at 100 Hz) at room temperature. The fluorescence was detected from the outset to 1 h at five minute intervals (see Fig. 8). The result showed that the fluorescence was enhanced uniformly with respect to time for the first 20 min, and reached a maximum value thereafter. It was assumed that, initially, the ultrasonication caused an increased chance of a valid collision occurring due to the dye molecules clustering together to form tiny

particles, and then the portion of the dye molecules remaining in the solvent mixture was gradually deposited onto the initially formed particles in a way similar to recrystallisation. Before 20 min had elapsed, compound **3a**, which dissolved in the solution, was precipitated completely; the fluorescence enhancement did not increase further. Thus, the size and orderliness between compound **3a** molecules in the aggregates can be increased in time: this was more propitious at enhancing restricted intramolecular rotation effects.

3.3. Crystal structure of **3a**

To understand what was happening in the aggregation, single crystals of **3a** was obtained by recrystallisation from methylene chloride and petroleum ether. The X-ray analysis of the crystals of **3a** (see Fig. 9) showed that the molecule was almost planar (the dihedral angle between the isatin ring and the phenyl ring was 4.5°) and had an intramolecular H-bond between the BF_2 group and the phenyl ring ($\text{C}-\text{H} \dots \text{F}$, 2.823 Å) that may further assist in restricting its rotation. The extended structure showed that **3a** adopted a head-to-tail one-dimensional arrangement along the crystallographic c-dimension (see Fig. 9) and the thus formed two-dimensional layers aggregated through $\pi-\pi$ interactions (4.125 and 4.353 Å) along the crystallographic b-dimension (see Fig. 9). The $\pi-\pi$ interaction between the isatinyl and phenyl rings of the two different molecules was most probably responsible for the red shift observed with the crystals of **3a** compared to its film.

Fluorophore, in this isatin-phenylhydrazone structure connected the isatin ring and aromatic moieties by rotatable N–N single bonds, exhibited free intramolecular rotation in the single molecule state, but this rotation was inhibited in the aggregated state. Because intramolecular rotation could be an effective mechanism for fluorescence quenching, such fluorophores generally show AIEE characteristics [17]. Strong AIEE effects were observed in these corresponding BF_2 complexes (**3**) due to the formation of a planar molecule with hydrazone moieties forming six-membered rings under the action of the BF_2 complex.

4. Conclusion

In conclusion, a new family of BF_2 -Hydrazone derivatives (**3**) containing isatin were developed that showed enhanced fluorescence upon their aggregation. In particular, these complexes displayed unusual aggregation-induced emission enhancement in the mixed solvent of THF/water or ethanol/water. Moreover, solvent- and time-influenced photoluminescence of AIEE in this mixture and

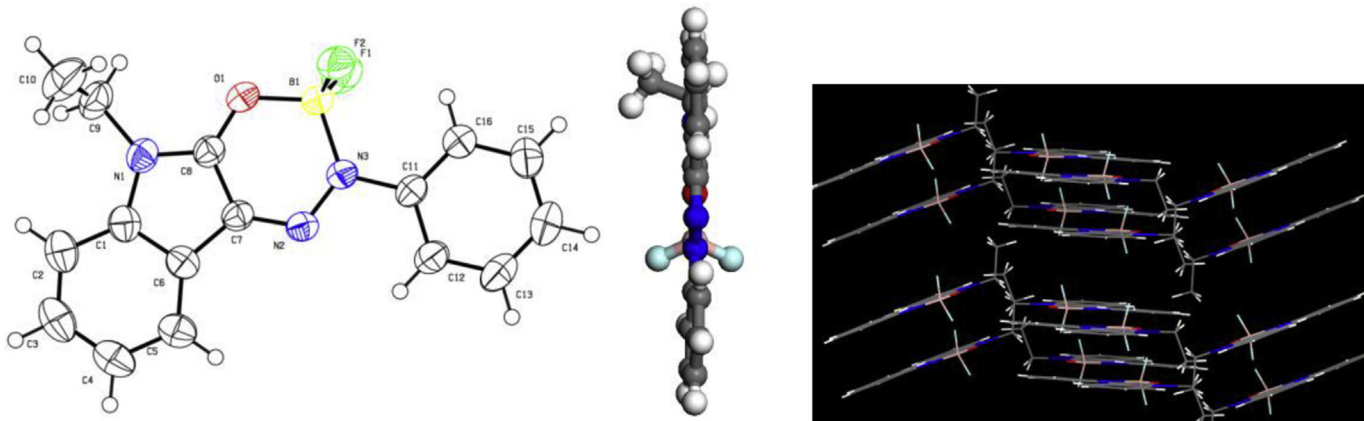


Fig. 9. Crystal structure of compound **3a** (CCDC 998356). Left: ORTEP drawing. Right: A 3D-stacking structure of **3a**.

solution for BODIHY **3** were observed and rationalised on the basis of X-ray crystallographic studies. These series of compounds could be applied to the design of OLEDs, live-cell imaging and fluorescent sensors.

Acknowledgement

We gratefully acknowledge the financial supported by the National Science Foundation of China (21176223) and the National Natural Science Foundation of Zhejiang (LY13B020016) and the Key Innovation Team of Science and Technology in Zhejiang Province (2010R50018).

References

- [1] (a) Harriman A, Mallon IJ, Stewart B, Ulrich G, Ziessel R. Boron dipyrromethene dyes bearing ancillary 2,2':6,2"-terpyridine coordination sites. *Ann Chem Pharm* 2007;19:3191–8;
- (b) Cao Q, Xiao SZ, Mao MF, Chen XH, Wang S, Li L, et al. Structure–property correlation of solid-emissive boron–fluorine derivatives. *J Organomet Chem* 2012;717:147–51;
- (c) Wang DF, Liu R, Chen C, Wang SF, Chang J, Wu CH, et al. Synthesis, photophysical and electrochemical properties of aza-boron-diquinomethene complexes. *Dyes Pigments* 2013;99:240–9;
- (d) Luo GG, Xia JX, Fang K, Zhao QH, Wu JH, Dai JC. Discovery of polymorphism-dependent emission for crystalline boron-dipyrromethene dye. *Dalton Trans* 2013;42:16268–71.
- [2] (a) Cihaner A, Algi F. A new conducting polymer bearing 4,4-difluoro-4-bora-3a,4a-diaza-s-indacene (BODIPY) subunit: synthesis and characterization. *Electrochim Acta* 2008;54:786–92;
- (b) Algi F, Cihaner A. An ambipolar low band gap material based on BODIPY and EDOT. *Org Electron* 2009;10:450–3.
- [3] (a) Yang F, Forrest SR. Photocurrent generation in nano structured organic solar cells. *ACS Nano* 2008;2:1022–32;
- (b) Rousseau T, Cravino A, Bura T, Ulrich G, Ziessel R, Roncali J. BODIPY derivatives as donor materials for bulk heterojunction solar cells. *Chem Commun* 2009;13:1673–5.
- [4] (a) Duro JA, de la Torre G, Barber J, Serrano JL, Torres T. Synthesis and liquid-crystal behavior of metal-free and metal-containing phthalocyanines substituted with long-chain amide groups. *Chem Mater* 1996;8:1061–6;
- (b) Olivier JH, Camerel F, Ulrich G, Barberá J, Ziessel R. Luminescent ionic liquid crystals from self-assembled BODIPY disulfonate and imidazolium frameworks. *Chem Eur J* 2010;16:7134–42;
- (c) Olivier JH, Barberá J, Bahaidarah E, Harriman A, Ziessel R. Self-Assembly of charged bodipy dyes to form cassettes that display intracomplex electronic energy transfer and accrete into liquid crystals. *J Am Chem Soc* 2012;134:6100–3.
- [5] (a) Emmelius M, Pawłowski G, Vollmann HW. Materials for optical data storage. *Angew Chem Int Ed* 1989;28:1445–71;
- (b) Cihaner A, Algi F. Synthesis and properties of 4,4-difluoro-4-bora-3a,4a-diaza-s-indacene (BODIPY)-based conducting copolymers. *React Funct Polym* 2009;69:62–7.
- [6] (a) Costela A, García-Moreno I, Pintado-Sierra M, Amat-Guerri F, Liras M, Sastre R, et al. New laser dye based on the 3-styryl analog of the BODIPY dye PM567. *J Photochem Photobiol A* 2008;198:192–9;
- (b) Bañuelos J, Martín V, Gómez-Durán CFA, Córdoba IJA, Peña-Cabrera E, García-Moreno I, et al. New 8-Amino-BODIPY derivatives: surpassing laser dyes at blue-edge wavelengths. *Chem Eur J* 2011;17:7261–70.
- [7] (a) Song Y, Di CA, Yang XD, Li SP, Xu W, Liu YQ, et al. A cyclic triphenylamine dimer for organic field-effect transistors with high performance. *J Am Chem Soc* 2006;128:15940–1;
- (b) Zhou Y, Lei T, Wang L, Pei J, Cao Y, Wang J. High-performance organic field-effect transistors from organic single-crystal microribbons formed by a solution process. *Adv Mater* 2010;22:1484–7;
- (c) Lu L, Yu FF, Long L, Yu JN, Wei B, Zhang JH, et al. Field effect transistor behavior of organic light-emitting diodes with a modified configuration of ITO anode. *Synth Met* 2010;160:2417–21;
- (d) Liu C, Minari T, Lu XB, Kumatanai A, Takimiya K, Tsukagoshi K. Solution-processable organic single crystals with bandlike transport in field-effect transistors. *Adv Mater* 2011;23:523–6;
- (e) Gholamrezaie F, Asadi K, Kicken RAJJ, Langeveld-Voss BMW, Leeuw DM, Blom PWM. Controlling charge injection by self-assembled monolayers in bottom-gate and top-gate organic field-effect transistors. *Synth Met* 2011;161:2226–9.
- [8] (a) Wu SD, Wang XY, Zhu CC, Song YJ, Wang J, Li YZ, et al. Monofunctional platinum complexes containing a 4-nitrobenzo-2-oxa-1,3-diazole fluorophore: distribution in tumour cells. *Dalton Trans* 2011;40:10376–82;
- (b) Tu WW, Lei JP, Wang P, Ju HX. Photoelectrochemistry of free-base-porphyrin-functionalized zinc oxide nanoparticles and their applications in biosensing. *Chem Eur J* 2011;17:9440–7;
- (c) Zhang XQ, Zhang XY, Yang B, Hui JF, Liu M, Chi ZG, et al. Facile preparation and cell imaging applications of fluorescent organic nanoparticles that combine AIE dye and ring-opening polymerization. *Polym Chem* 2014;5:318–22.
- [9] (a) Mishra A, Periasamy N, Patankar MP, Narasimhan KL. Synthesis and characterisation of soluble aluminium complex dyes based on 5-substituted-8-hydroxyquinoline derivatives for OLED applications. *Dyes Pigments* 2005;66:89–97;
- (b) Zhao J, Yu JS, Ma Z, Li L, Jiang YD. Optimization of yellow phosphorescent organic light-emitting devices based on triplet exciton diffusion length. *Synth Met* 2011;161:2417–21;
- (c) Li HY, Chi ZQ, Zhang XQ, Xu BQ, Liu SW, Zhang Y, et al. New thermally stable aggregation-induced emission enhancement compounds for non-doped red organic light-emitting diodes. *Chem Commun* 2011;47:11273–5;
- (d) Gao CH, Zhou DY, Gu W, Shi XB, Wang ZK, Liao LS. Enhancement of electroluminescence efficiency and stability in phosphorescent organic light-emitting diodes with double exciton-blocking layers. *Org Elect* 2013;14:1177–82.
- [10] (a) Huang XH, Gu XG, Guanxin Zhang GX, Zhang DQ. A highly selective fluorescence turn-on detection of cyanide based on the aggregation of tetraphenylethylene molecules induced by chemical reaction. *Chem Commun* 2012;48:12195–7;
- (b) Zhou QX, Lei WH, Chen YJ, Li C, Hou YJ, Zhang BW. Ruthenium(II)-arene complexes with strong fluorescence: insight into the underlying mechanism. *Chem Eur J* 2012;18:8617–21;
- (c) Bardajee GR. Microwave-assisted solvent-free synthesis of fluorescent naphthalimide dyes. *Dyes Pigments* 2013;99:52–8;
- (d) Staneva D, Bosch P, Asiri AM, Taib LA, Grabchev I. Studying pH dependence of the photophysical properties of a blue emitting fluorescent PAMAM dendrimer and evaluation of its sensor potential. *Dyes Pigments* 2014;105:114–20.
- [11] (a) Luo JD, Xie ZL, Lam JWY, Cheng L, Chen HY, Tang BZ, et al. Aggregation-induced emission of 1-methyl-1,2,3,4,5-pentaphenylsilole. *Chem Commun* 2001;18:1740–1;
- (b) Li Z, Dong YQ, Mi BX, Tang YH, Tong H, Tang BZ, et al. Structural control of the photoluminescence of silole regioisomers and their utility as sensitive regiodiscriminating chemosensors and efficient electroluminescent materials. *J Phys Chem B* 2005;109:10061–6;
- (c) Tong H, Hong YN, Dong YQ, Häußler M, Lam JWYL, Tang BZ, et al. Fluorescent “light-up” bioprobes based on tetraphenylethylene derivatives with aggregation-induced emission characteristics. *Chem Commun* 2006;35:3705–7;
- (d) Zhao ZJ, Chen SM, Shen XY, Mahtab F, Yu Y, Tang BZ, et al. Aggregation-induced emission, self-assembly, and electroluminescence of 4,4'-bis(1,2,2-triphenylvinyl)biphenyl. *Chem Commun* 2010;46:686–8.
- [12] (a) Hong YN, Lama JWY, Tang BZ. Aggregation-induced emission: phenomenon, mechanism and applications. *Chem Commun* 2009;29:4332–53;
- (b) Quan L, Chen Y, Lv XJ, Fu WF. Aggregation-induced photoluminescent changes of naphthyridine-BF₂ complexes. *Chem Eur J* 2012;18:14599–604;
- (c) Yang Y, Su X, N.Carroll C, Aprahamian I. Aggregation-induced emission in BF₂-hydrazone (BODIHY) complexes. *Chem Sci* 2012;3:610–3;
- (d) Chen WD, Zhang DW, Gong WT, Lin Y, Ning GL. Aggregation-induced emission of a novel conjugated phosphonium salt and its application in mitochondrial imaging. *Spectrochim Acta A* 2013;110:471–3;
- (e) Xie YZ, Shan GG, Li P, Zhou ZY, Su ZM. A novel class of Zn(II) Schiff base complexes with aggregation-induced emission enhancement (AIEE) properties: synthesis, characterization and photophysical/electrochemical properties. *Dyes Pigments* 2013;96:467–74;
- (f) Sharma S, Dhir A, Pradeep CP. ESIPt induced AIEE active material for recognition of 2-thiobarbituric acid. *Sens Actuat B Chem* 2014;191:445–9.
- [13] Bhongale CJ, Chang CW, Lee CS, Diau EWG, Hsu CS. Relaxation Dynamics and structural characterization of organic nanoparticles with enhanced emission. *J Phys Chem B* 2005;109:13472–82.
- [14] Chen JW, Peng H, Law CCW, Dong YP, Lam JWY, Williams ID, et al. Hyper-branched poly(phenylenesilolene)s: synthesis, thermal stability, electronic conjugation, optical power limiting, and cooling-enhanced light emission. *Macromolecules* 2003;36:4319–27.
- [15] Wang F, Han MY, Mya KY, Wang Y, Lai YH. Aggregation-driven growth of size-tunable organic nanoparticles using electronically altered conjugated polymers. *J Am Chem Soc* 2005;127:10350–5.
- [16] Itami K, Ohashi Y, Yoshida JI. Triarylethene-based extended π-systems: programmable synthesis and photophysical properties. *J Org Chem* 2005;70:2778–92.
- [17] Tang WX, Xiang Y, Tong A. Salicylaldehyde azines as fluorophores of aggregation-induced emission enhancement characteristics. *J Org Chem* 2009;74:2163–6.
- [18] (a) Jenekhe SA, Osaheni JA. Excimers and exciplexes of conjugated polymers. *Science* 1994;265:765–8;
- (b) Friend RH, Gymer RW, Holmes AB, Burroughes JH, Marks RN, Taliani C, et al. Electroluminescence in conjugated polymers. *Nature* 1999;397:121–8;
- (c) Babel A, Jenekhe SA. Electron transport in thin-film transistors from an n-type conjugated polymer. *Adv Mater* 2002;14:371–4;
- (d) Toal SJ, Jones KA, Magde D, Troglar WC. Luminescent silole nanoparticles as chemoselective sensors for Cr(VI). *J Am Chem Soc* 2005;127:11661.

- [19] (a) Shirai K, Matsuoka M, Fukunishi K. Fluorescence quenching by intermolecular π - π interactions of 2,5-bis(N,N-dialkylamino)-3,6-dicyanopyrazines. *Dyes Pigments* 1999;42:95–101;
(b) Shirai K, Matsuoka M, Matsumoto S, Shiro M. Molecular stacking and solid state spectra of 2,5-bis(1-aza-1-cycloalkyl)-3,6-dicyanopyrazines and their X-ray crystal structures. *Dyes Pigments* 2003;56:83–7;
(c) Ooyama Y, Okamoto T, Yamaguchi T, Suzuki T, Hayashi A, Yoshida K. Heterocyclic quinol-type fluorophores: synthesis, X-ray crystal structures, and solid-state photophysical properties of novel 5-hydroxy-5-substituent-benzo[b]naphtho[1,2-d]furan-6-one and 3-hydroxy-3-substituent-benzo[*kl*]xanthene-2-one derivatives. *Chem Eur J* 2006;12:7827–38;
(d) Park SY, Ebihara M, Kubota Y, Funabiki K, Matsui M. The relationship between solid-state fluorescence intensity and molecular packing of coumarin dyes. *Dyes Pigments* 2009;82:258–67.
- [20] Chen G, Liu B, Tang Y, Deng Q, Hao XJ. Synthesis and novel crystal structure of (E, Z) 3-aminomethylene-1-ethyl-indol-2-one. *Heterocycl Commun* 2010;16: 25–32.
- [21] Ellis JM, Overman LE, Tanner HR, Wang J. A versatile synthesis of unsymmetrical 3,3'-bioindoles: stereoselective mukaiyama aldol reactions of 2-siloxindoles with isatins. *J Org Chem* 2008;73:9151–4.
- [22] Hajare RA, Gaurkhede RM, Chinhole PP, Chandewar AV, Wandhare AS, Karki SS. Synthesis, structure and spectral characterization of Friedel crafts N-benzylation of isatin and their novel Schiff's bases. *Asian J Res Chem* 2009;2: 289–91.
- [23] Li HY, Chi ZQ, Zhang XQ, Xu BQ, Liu SW, Zhang Y, et al. New thermally stable aggregation-induced emission enhancement compounds for non-doped red organic light-emitting diodes. *Chem Commun* 2011;47:11273–5.
- [24] (a) Kamino S, Horio YK, Komeda S, Minoura K, Ichikawa H, Horigome J, et al. A new class of rhodamine luminophores: design, syntheses and aggregation-induced emission enhancement. *Chem Commun* 2010;46:9013–5;
(b) Liang ZQ, Li YX, Yang JX, Ren Y, Tao XT. Suppression of aggregation-induced fluorescence quenching in pyrene derivatives: photophysical properties and crystal structures. *Tetrahedron Lett* 2011;52:1329–33.